ANL/CP--76029

DE92 015222

ANALYSIS OF EROSION AND TRANSPORT OF CARBON IMPURITY IN THE TFTR INNER BUMPER LIMITER REGION

by

T. Q. Hua and J. N. Brooks
Engineering Physics Division
Argonne National Laboratory
9700 South Cass Avenue
Argonne, IL 60439

Presented at the 10th International Conference on Plasma Surface Interactions in controlled fusion devices, March 30 - April 3, 1992, Monterey, CA.

ANALYSIS OF EROSION AND TRANSPORT OF CARBON IMPURITY IN THE TFTR INNER BUMPER LIMITER REGION*

T. Q. Hua and J. N. Brooks
Engineering Physics Division
Argonne National Laboratory
9700 South Cass Avenue
Argonne, IL 60439

Abstract

Carbon sputtering and transport on the TFTR inner graphite bumper limiter is investigated with the impurity transport code REDEP. Analysis is carried out for a series of ohmic discharges in TFTR. Predictions for Z_{eff} in the core plasma agree well with in-situ experimental measurements. Run-away self-sputtering of carbon is predicted at low densities and high edge plasma temperatures when the limiter surface was purged of deuterium. Surface erosion and deposition is analyzed. In general, redeposition reduces the peak erosion by about a factor of five. Analysis is also carried out for a typical neutral beam heated discharge with a noncircular plasma. Spatial surface erosion and deposition profiles are compared qualitatively with beta backscattering measurements of metal deposition found on the limiter.

---

*Work supported by the U.S. DOE/Office of Fusion Energy

I. Introduction

The feasibility of tokamak operation depends strongly on the control of impurity generation and transport in the edge region. Plasma contamination could result in significant radiative power loss or disruption. Surface erosion by sputtering limits the lifetime of plasma facing components such as a limiter and divertor in a tokamak reactor.

Surface erosion and redeposition on the TFTR inner bumper limiter has been previously investigated[1] with the REDEP code [2]. The results for surface erosion and deposition compared favorably with in-situ beta backscattering measurements of metal deposition after several thousand discharges during the run period from October 1985 through June 1987. The REDEP code has also been benchmarked with the ALT-I limiter heads in TEXTOR[3], and recently with the DIII-D divertor[4]. The comparisons are good, but ongoing additional validation is required, particularly on a shot-to-shot basis.

The bumper limiter was realigned in 1989 to obtain more uniform heat loading and to correct earlier alignment problems. In this study, the new configuration of the limiter was modelled in a 3-D analysis of impurity generation and transport using the REDEP code. Ten ohmic shots selected from a controlled sequence of ohmic discharges in TFTR were analyzed. Plasma parameters needed for inputs to REDEP were taken from experimentally measured and/or deduced data[5]. These include edge plasma density, temperature, incident deuterium flux, and associated e-folding lengths.

Calculated magnetic flux surfaces, slightly noncircular for ohmic shots and elliptical for neutral beam heated discharges, were used in determining incident plasma flux on the limiter and following impurity transport. Self-sputtering coefficients for both pure C and hydrogen saturated C were used to simulate the ohmic shots under various plasma conditions.

II. Modelling

II.A. The REDEP Code

Details of the code have been described elsewhere[2], and only briefly here. The code calculates the erosion and redeposition of material due to sputtering from a limiter or divertor surface. Sputtering mechanisms include physical, chemical, and radiation enhanced sublimation. For the TFTR conditions presented here, only physical sputtering occurs. Impurity transport into and out of the core plasma is also modelled.

Sputtering models used for the calculations are as follows. Deuterium ions and charge exchange neutrals impinge on the surface with average incidence angles (from the normal) of 60° and 45°, respectively. Carbon neutrals that are ionized in the scrape off zone return to the limiter with average charge state +3 while carbon ions diffusing from the core are fully stripped of electrons [6]. Sheath calculations[7] were made for a DT plasma containing C^{+3} and C^{+6} ions to determine the average incidence angles for the returning carbon ions. Edge conditions of $n_e=5\times10^{18}$ m^{-3} , $T_e=T_i=100$

eV, B=5T, and ψ=85° were used (ψ is the field line angle from the surface normal). Although ψ ~ 89° for the TFTR bumper limiter, the sheath code was not run for ψ > 85° because of numerical reasons. In the present calculations we have used the ψ=85° results which gave average incidence angle of 60° for C^{+6} and 50° for C^{+3} ions.

Sputtered neutrals were launched with an angular cosine distribution and velocity determined from the random collision cascade mode[8]. Self-sputtering coefficients for pure C were computed by multiplying the normal incidence yields[9] by an angular enhancement factor[10]. The normal incidence self-sputtering yields were multiplied by 0.9 so as to better match available experimental data. Self sputtering coefficients for hydrogen saturated carbon were computed using the model described in ref. 6. This model predicts a reduction in carbon sputtering for hydrogen containing carbon compared to "pure" carbon. It should be noted, however, that there is little or no experimental data on oblique incidence self-sputtering coefficients of hydrogen saturated carbon.

II.B. Limiter Geometry

The TFTR inner bumper limiter provides complete toroidal coverage of the inner wall and poloidal coverage of ± 60° from the torus midplane. There are 20 toroidal sectors, and each sector is mounted with 96 carbon tiles arranged into 4 columns and 24 rows. In our model, each tile is divided into 4 elements: 2 each in the toroidal and poloidal directions. Figure 1 shows the configuration

of 1 sector with a total of 384 elements. The dimensions of the tiles and their mounting locations are inputs to the engineering finite element code PATRAN™[11] to produce a PATRAN™ data file which is linked to REDEP for analysis. This data file contains the necessary spatial information for all elements and nodes making up the limiter, and the connection of elements to corner nodes, of nodes to adjacent elements. PATRAN™ was also used to generate color displays of the calculated erosion/deposition profiles as well as the measured metal deposition on the limiter.

II.C. Shadowing

The installation and machining of the tiles produce a slight deviation from toroidal symmetry. As a result, within a sector, most of the top right quadrant as seen from the plasma side is shadowed by the top left quadrant, and most of the bottom left quadrant is shadowed by the bottom right quadrant. Shadowed elements are determined by launching a field line from the center of every element and following that field line to see if it clears the adjacent limiter sector. Unshadowed elements therefore receive direct incident flux from the plasma while shadowed elements receive plasma flux through radial diffusion across magnetic flux surfaces. The average connection length is greater than 50 m for unshadowed elements but less than 0.5 m for shadowed elements. In impurity transport analysis, the edge plasma scrape-off length is assumed to be proportional to the square root of the connection length, so in the present analysis e-folding lengths for shadowed

elements are reduced by a factor of ten.

II.D. Magnetic Field

Magnetic flux surfaces were calculated for both ohmic and neutral beam discharges[12]. They are slightly noncircular for ohmic discharges and elliptical for beam heated discharges. The field lines make a toroidal pitch angle of about 2° from upper left to lower right. The field data file contains 7 flux surfaces for a given set of plasma conditions. Each flux surface is comprised of poloidal and toroidal field components at 100 discrete points. The last closed flux surface making first contact with the limiter was interpolated from the two innermost flux surfaces(fig. 2).

At the center of each element a unit tangent vector of the field is calculated to compute the incident particle flux according to

$$\Gamma(x) = \Gamma_o \, e^{-x/\lambda_\Gamma} \, \hat{\underset{\sim}{b}} \cdot \hat{\underset{\sim}{n}}$$

where Γ_o is the parallel particle flux at the last closed flux surface, x is the radial distance form the center of the element to the last closed flux surface, λ_Γ is the e-folding length, and $\hat{\underset{\sim}{n}}$ is the surface normal unit vector. Once a sputtered neutral is ionized in the scrape-off zone, a magnetic field line crossing the point of ionization is traced out to determine where the ion is subsequently redeposited.

III. Results And Discussions

The dependence of plasma boundary conditions on the central density has been investigated in a controlled sequence of ohmic discharges in TFTR with constant input power of about 1 MW[5]. Plasma boundary behaviors were experimentally measured with various diagnostics including reciprocating Langmuir probes, poloidal D_α, $C_{//}$ arrays. The average plasma density, $\langle n_e \rangle$, was varied from 1×10^{19} m^{-3} to 4×10^{19} m^{-3} . Ten selective shots, which span the range of density, from that series were analyzed. Experimental data such as plasma edge electron density, temperature, e-folding lengths and deuterium parallel flux were used as inputs to REDEP. Table I summarizes the relevant parameters.

Each of the ten ohmic shots was analyzed assuming pure C material and repeated for hydrogen saturated C (H/C=0.4) which, in theory, has lower sputtering yields. The presence of C impurity in the core resulted in Z_{eff} greater than unity. Figure 3 compares the predicted values for Z_{eff} with experimental measurements. The predicted values for hydrogen-saturated carbon tiles agree very well with experiment for $\langle n_e \rangle \geq 1.5 \times 10^{19}$ m^{-3} . At the lowest density, $\langle n_e \rangle \approx 1 \times 10^{19}$ m^{-3} REDEP predicted $Z_{eff} \approx 2.1$ while experiment showed a sharp increase over a wide range from 2.5 - 4.6. In the experiment, the lowest deuterium density was determined by the carbon recycling limit, i.e., the limiter was purged of deuterium such that Γ_D falls to zero and the density was maintained by carbon self-sputtering. Therefore at low density, calculations for pure C tiles should provide a more reasonable

description of the depletion of hydrogen concentration in graphite. Under these conditions, the computed carbon self-sputtering coefficients due to plasma impurity flux exceeded unity at elements near the limiter midplane. As a result, a large influx of carbon impurity could be expected. This finding is consistent with experimental observation. Fig. 4, reproduced from Ref. 5, shows the deuterium and carbon currents to the limiter. For values of $\langle n_e \rangle > 1.5 \times 10^{19}$ m^{-3} I_C increases with increasing I_D, but at $\langle n_e \rangle \approx 1 \times 10^{19}$ m^{-3} a sharp burst of I_C was detected reflecting the sharp increases in Z_{eff}. Since the steady state REDEP solution is unstable when the sputtering coefficients exceed unity, the predicted Z_{eff} for pure C in fig. 2 at the lowest density were included only to represent the run-away situations. At higher densities and lower temperatures, the sputtering coefficients never exceeded unity.

One other modeling issue is worth briefly noting. The angular incidence angle is a key element in the sputtering model because C sputtering yields are enhanced at increasingly glancing angles up to a limit near 90° when the effects of microstructure, e.g. cone formation could mitigate the effects of glancing impingement angle. In reality, there is a distribution of incidence angles, in REDEP the average value of such a distribution is used. To illustrate the effect of incidence angle on sputtering yields, the calculations were repeated using an incidence angle of 50° for C^{+6} impinging on pure C. The computed self-sputtering coefficients in these cases were less than unity everywhere. Convergence of

solutions were achieved giving $Z_{eff} \approx 3.1$ at the low density limit. It is quite possible that run-away of self-sputtered carbon could occur if the sputtering model uses a distribution of incidence angles averaged at 50° but with nontrivial probability for angles over 60°. Sheath code analysis of this subject is being planned to develop better estimates of the incident angle.

III. B. Erosion/Deposition Profiles

The peak net erosion is about a factor of 5 lower than the peak gross erosion. The erosion/deposition profiles for shot 45434 is shown in Fig. 5. Negative net erosion rates imply net growth. By symmetry, analysis was carried out for the top limiter half, results were reflected to the bottom half, and plotted for the whole sector. There is a net migration of sputtered carbon from regions with large plasma fluxes (top left and bottom right quadrants) to regions where fluxes are lower (top right and bottom left quadrants).

During the 1990 vessel opening, the areal density of metal impurities deposited on the limiter was mapped in-situ using beta backscattering[13]. The mapping density was sparse, i.e., less measurements were taken, compared to the 1987 mapping[14]. However the metal deposition patterns were very similar[13]. Shown in Fig. 6 is the detailed pattern mapped during the 1987 vessel opening. Ex-situ surface analysis of tiles removed from the limiter showed strong correlation between metal film thickness to the co-deposited carbon layer. Regions with low metal deposition had shiny

footprints indicating carbon erosion and high plasma flux, and regions with high metal concentration corresponds to carbon deposition. Comparison of figs. 5 and 6 gives satisfactory qualitative agreement.

A typical neutral beam discharge was also analyzed for H-saturated C with $n_e(a)=5x10^{19}$ m^{-3} , $T_e(a)=200$ eV, $\lambda_n=0.04$ m and $\lambda_T=0.045$ m. Results are shown in fig. 7. Notice that deposition was also predicted at the area just to the left of the poloidal midline dividing the top left and top right quadrants. In fig. 5 there is net erosion there while beta backscattering data in fig. 6 shows deposition.

IV. Conclusions

Analysis has been carried out to model carbon sputtering and transport on the TFTR bumper limiter. The calculations for a series of ohmic discharges predict self-sputtering run-away in pure C for shots at low densities ($\langle ne\rangle \approx 1x10^{19}$ m^{-3}) and high edge temperatures (50-60 eV). The predictions are consistent with experimental observation. A key element contributing to the run-away is the off-normal incidence angle of C^{+6} ions. A reduction of the average angle used in the calculations from 60° to 50° would result in no run-away of carbon. Another important factor is the energy acquired by the ions traversing the sheath for the very oblique magnetic field. Since sheath calculations to-date have not been performed for TFTR conditions at field angles greater than 85°, further analysis is needed to provide better boundary

conditions and information to plasma transport codes and impurity transport code like REDEP. A comparison of predicted carbon erosion profiles with measured metal deposition profiles shows satisfactory qualitative agreement. In general, there is a net migration of sputtered carbon material from regions with large plasma fluxes to regions with low fluxes.

Acknowledgments

The authors wish to thank Dr. M. Ulrickson of PPPL for providing the limiter construction and magnetic field data as well as useful discussions, Dr. R. McGrath of Sandia, Albuquerque for introducing the PATRAN™ code and helpful discussions, Dr. B. Mills of Sandia, Livermore for the beta backscattering data, and Dr. C. S. Pitcher of the Univ. of Toronto for the ohmic shots edge plasma parameters.

References

1. R. T. McGrath and J. N. Brooks, J. Nucl. Mater. 162-164 (1989) 350.

2. J. N. Brooks, Nucl. Technol./Fusion, 4, (1983) 33.

3. R. T. McGrath et al., J. Nucl. Mater., 145-147, (1987) 660.

4. C. P. C. Wong et al., 10th Int. Conf. on Plasma Surface Interactions in Controlled Fusion Devices (1992).

5. C. S. Pitcher, P. C. Stangeby, R. V. Budny et al., Nuclear Fusion (1992).

6. C. D. Boley and J. N. Brooks, FED/INTOR/ICFW182-16, Chap VI, Georgia Inst. of Tech. (1982).

7. J. N. Brooks, D. K. Brice, A. B. Dewald, and R. T. McGrath, J. Nucl. Mater. 162-164 (1989) 363.

8. N. Thompson, Philos. Mag. 18, (1968) 377.

9. N. Matsunami et al., Atomic Data and Nuclear Tables, 31, 1(1984).

10. Y. Yamamura, Y. Itikawa, and N. Itoh, IPPF-AM-26 (inst. Plasma Phys. Nagoya Univ.) (1983).

11. PATRAN™-G, PDA Engineering, Costa Mesa, California.

12. M. Bell, PPPL, Private Communication (1991).

13. B. Mills, Sandia National Labs, Private Communication (1992).

14. W. R. Wampler et al., J. Vac. Sci. & Technol.-A, 6, (1988) 2111.

Table 1. Edge Plasma Parameters for a Series of Ohmic Discharges in TFTR.

Shot No.	$\langle n_e \rangle$ $\times 10^{19} m^{-3}$	$n_e(a)$ $\times 10^{19} m^{-3}$	$T_e(a)$ eV	λ_n $\times 10^{-2} m$	λ_n $\times 10^{-2} m$	λ_Γ^* $\times 10^{-2} m$
45421	1.07	0.23	48.0	6.8	9.5	5.0
45423	1.09	0.28	58.0	5.7	6.4	3.9
45424	1.08	0.26	55.0	6.8	5.5	4.2
45425	1.50	0.37	45.0	4.7	6.1	3.4
45426	1.48	0.35	51.0	4.6	5.4	3.2
45432	1.08	0.25	50.5	6.7	7.4	4.6
45434	2.05	0.60	35.0	4.0	13.0	3.5
45435	2.69	0.75	22.0	3.6	14.4	3.2
45438	3.92	1.20	28.0	4.0	8.2	3.2
45470	3.68	1.25	24.0	4.1	14.5	3.6

* particle flux e-folding distance is calculated from

$$\frac{1}{\lambda_\Gamma} = \frac{1}{\lambda_n} + \frac{1}{2\lambda_T}$$

List Of Figures

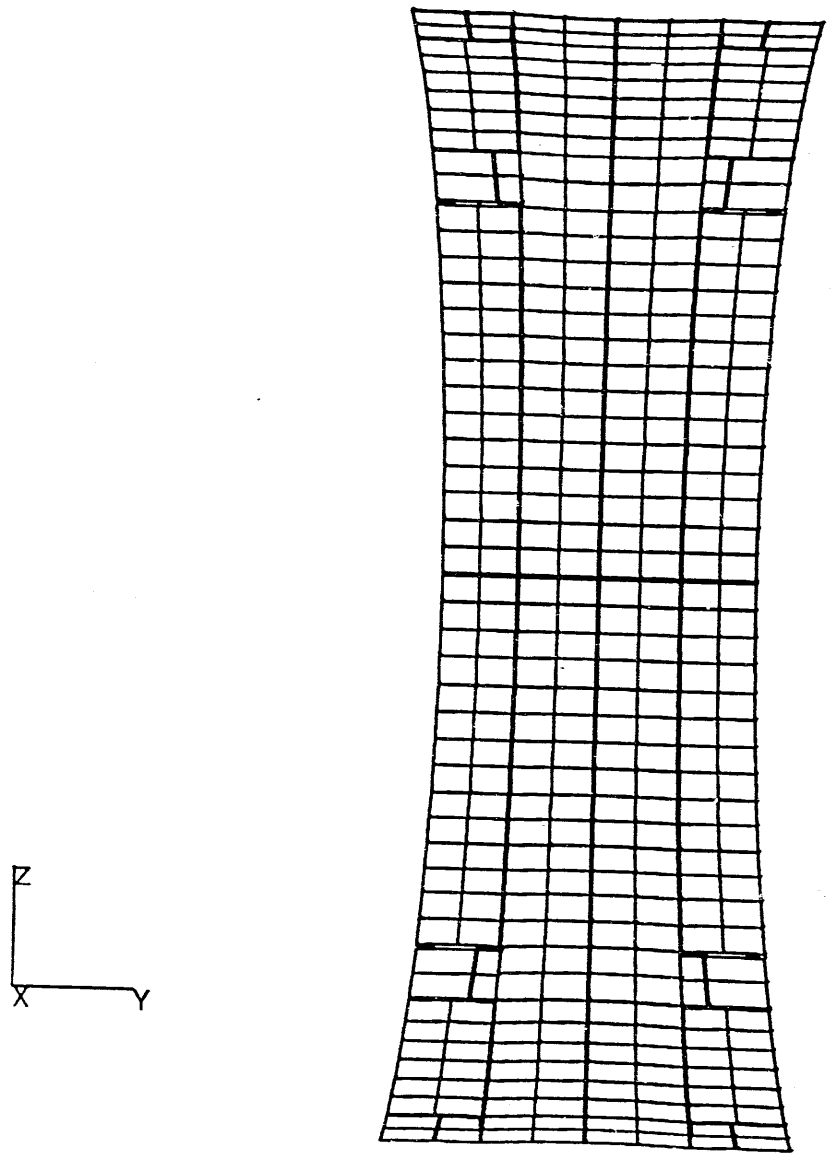

Fig. 1

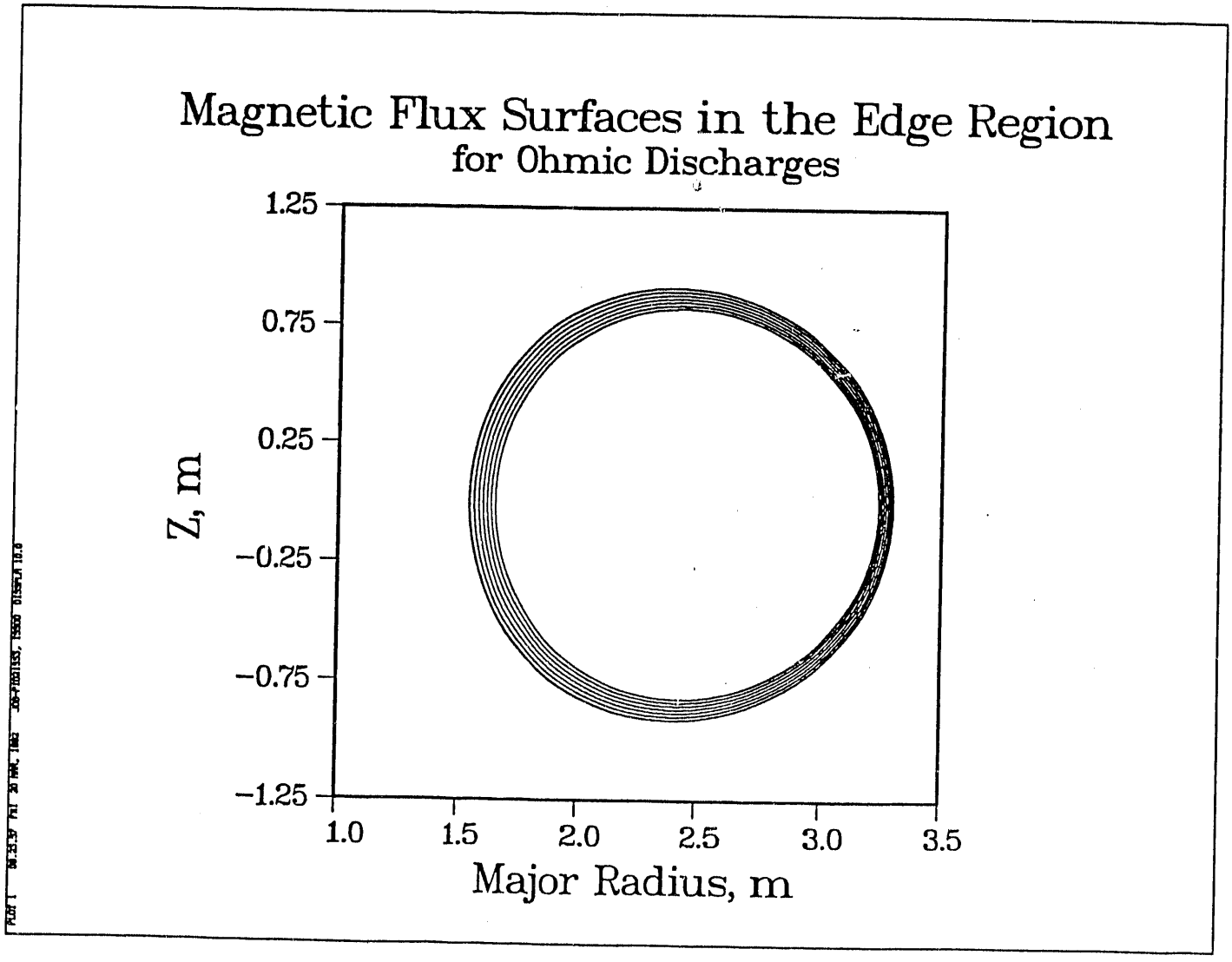
Magnetic Flux Surfaces in the Edge Region
for Ohmic Discharges
1.25
0.75
0.25
−0.25
−0.75
−1.25
Z, m
1.0
1.5
2.0
2.5
3.0
3.5
Major Radius, m

Fig. 2a

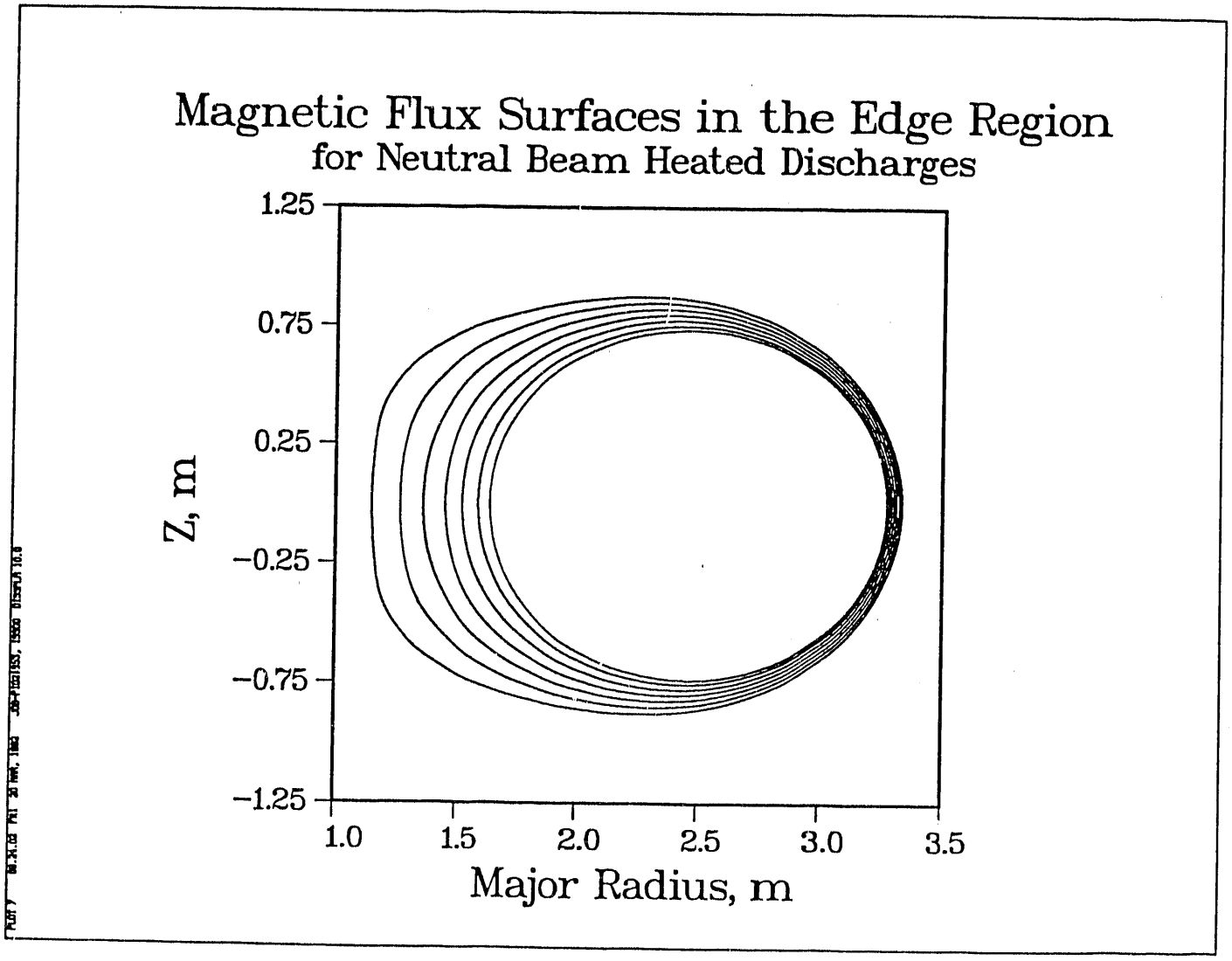
Magnetic Flux Surfaces in the Edge Region
for Neutral Beam Heated Discharges
1.25
0.75
0.25
−0.25
−0.75
−1.25
Z, m
1.0
1.5
2.0
2.5
3.0
3.5
Major Radius, m

Fig. 2b

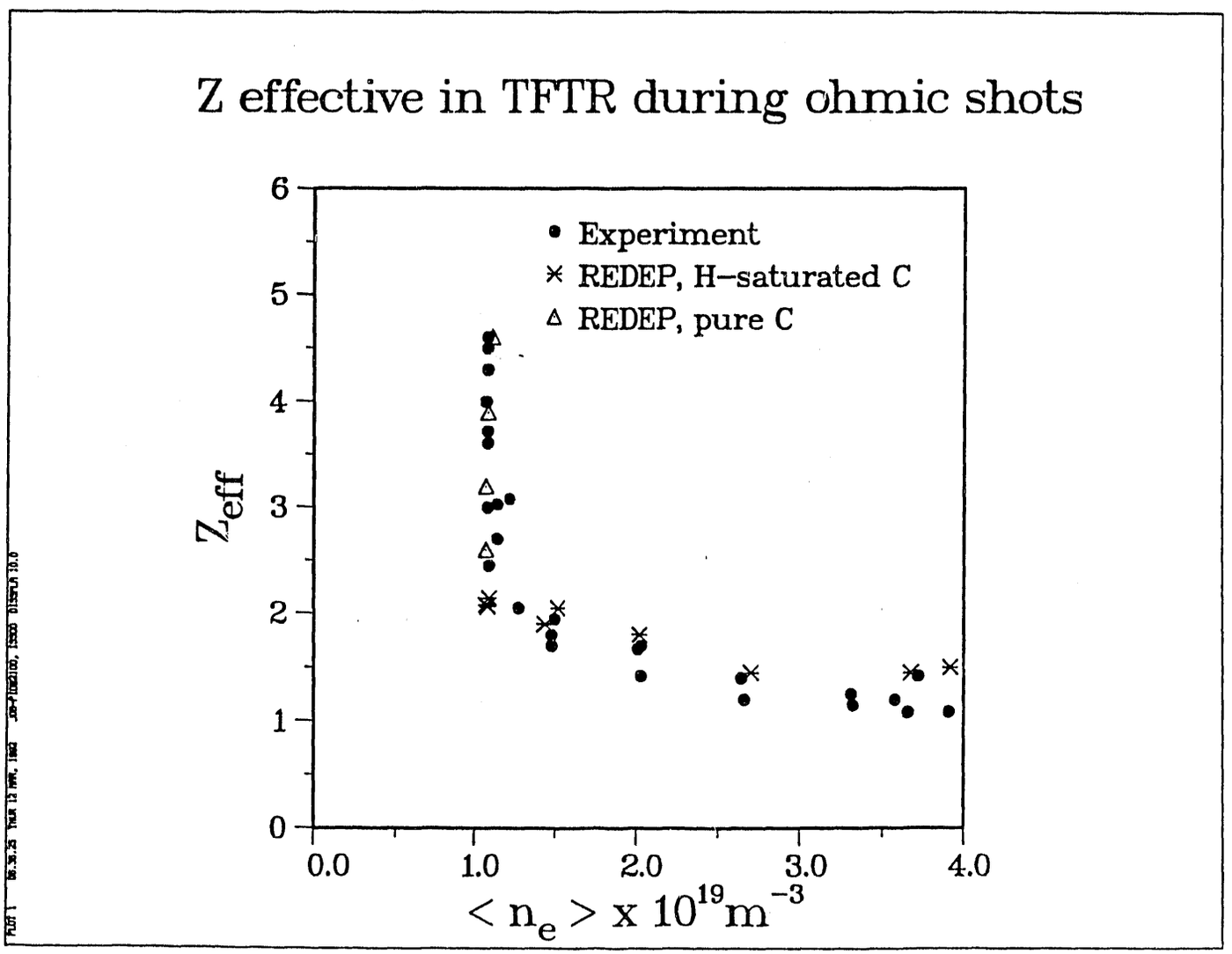
Z effective in TFTR during ohmic shots
Experiment
REDEP, H–saturated C
REDEP, pure C
Z_{eff}
$< n_e > x\ 10^{19} m^{-3}$
0
1
2
3
4
5
6
0.0
1.0
2.0
3.0
4.0

Fig. 3

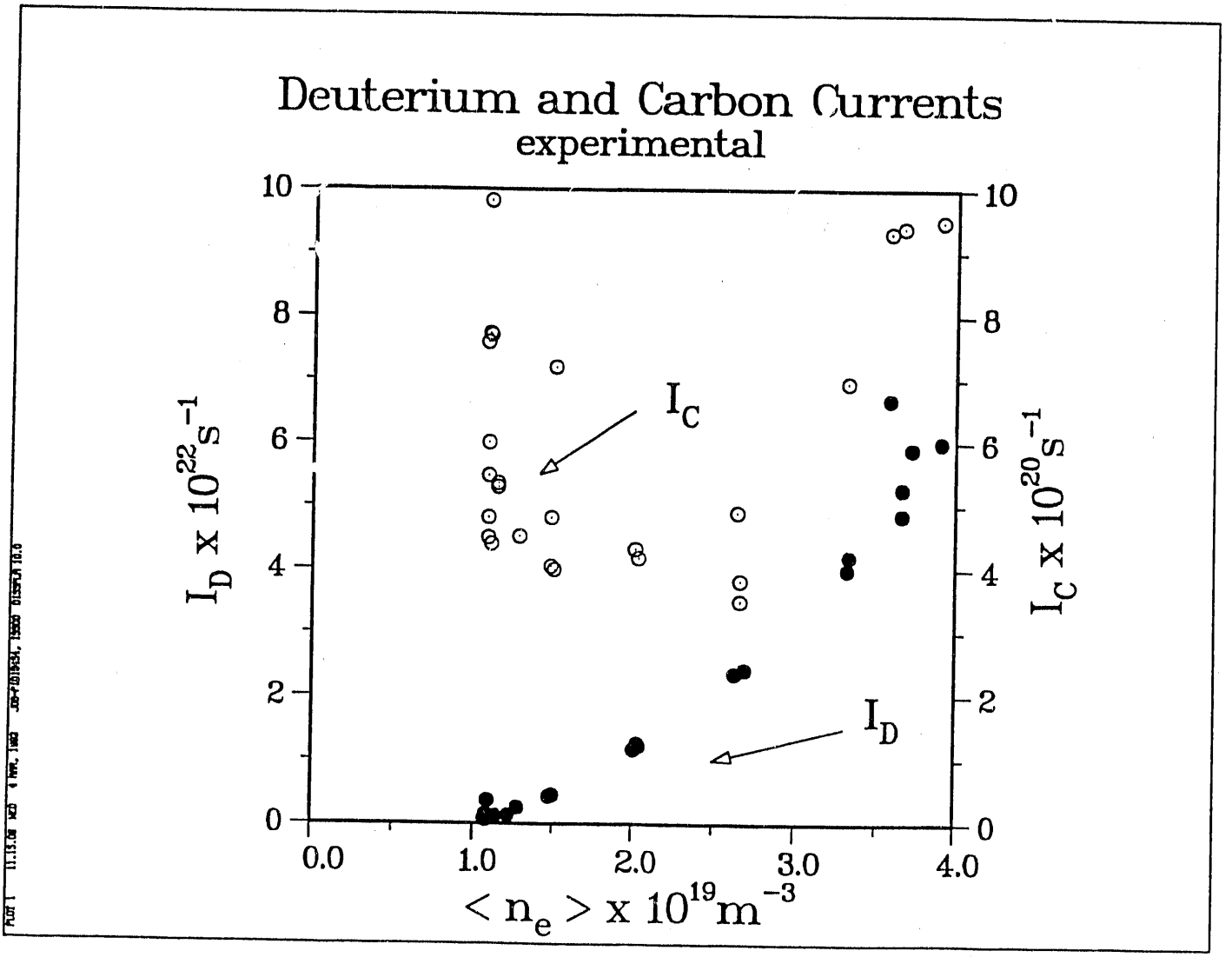
Deuterium and Carbon Currents
experimental
I_D x 10^{22} s^{-1}
I_C x 10^{20} s^{-1}
I_C
I_D
$< n_e >$ x 10^{19} m^{-3}
0.0
1.0
2.0
3.0
4.0
0
2
4
6
8
10

Fig 4

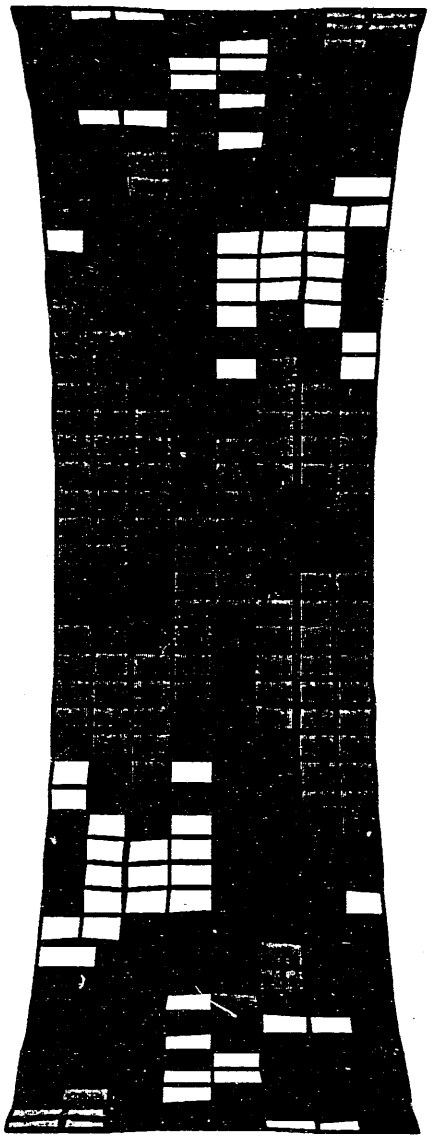

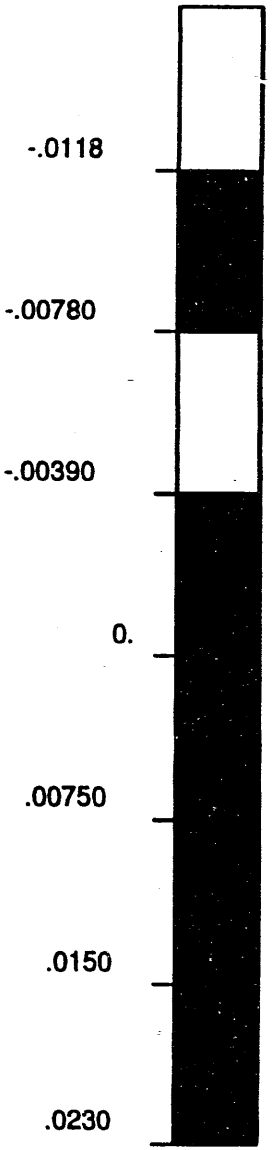

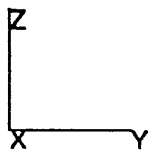

EROSION RATES(ANG/S)
TFTR5.ELS

Fig 5

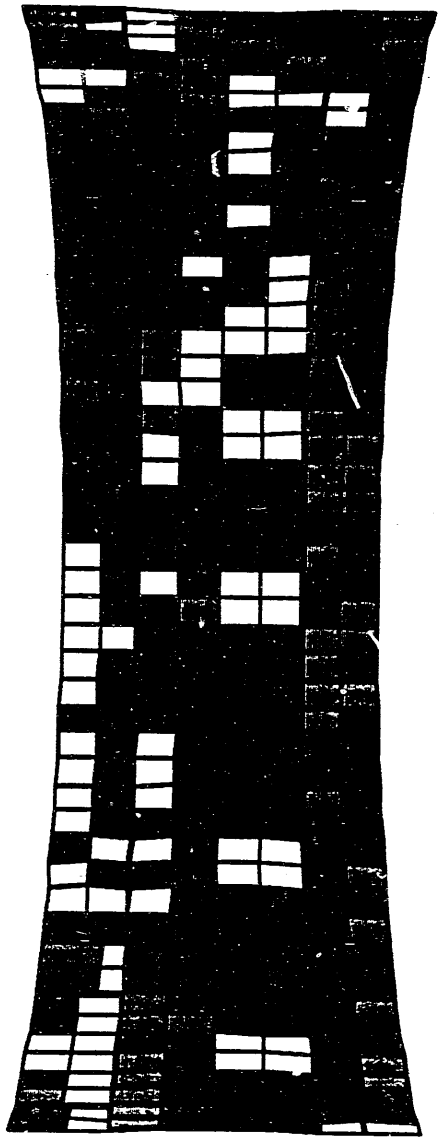

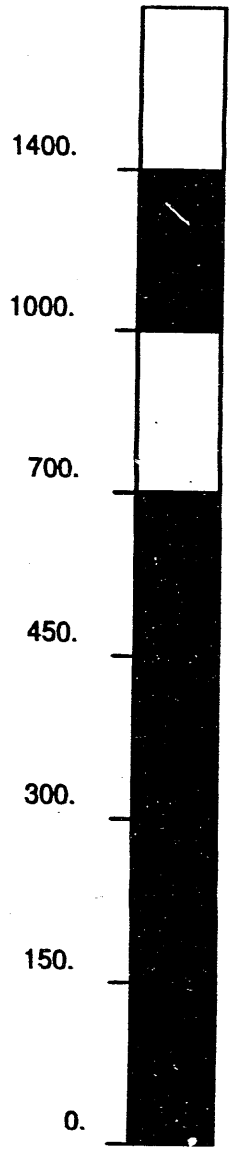

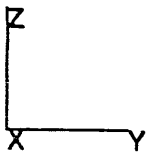

METAL DEPOSIT
BETA BACKSCATTERING

Fig 6

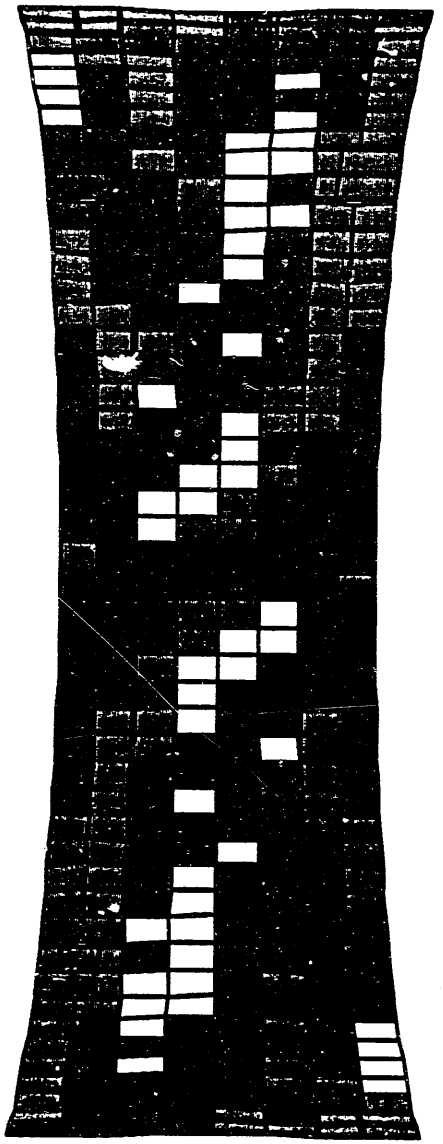

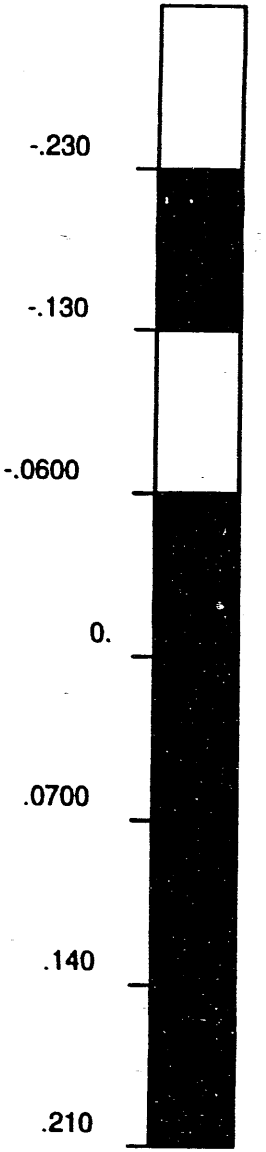

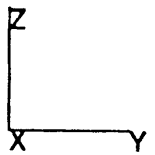

EROSION RATE(ANG/S)
TFTR6.ELS
NBI

Fig. 7

END

DATE FILMED

8/11/92